Journal of Power Sources 248 (2014) 752–761

Contents lists available at ScienceDirect

Journal of Power Sources

journal homepage: www.elsevier.com/locate/jpowsour

Sulfur infiltrated activated carbon cathodes for lithium sulfur cells: The combined effects of pore size distribution and electrolyte molarity

Jung Tae Lee [a], Youyang Zhao [a], Hyea Kim [a], Won Il Cho [b], Gleb Yushin [a,*]

[a] School of Materials Science and Engineering, Georgia Institute of Technology, Atlanta, GA 30332, USA
[b] Energy Storage Research Center, National Agenda Research Division, Korea Institute of Science and Technology, Cheong Ryang, Seoul 130-650, South Korea

HIGHLIGHTS

- At 25 °C, microporous S-activated carbon (AC) exhibited small capacity.
- At 70 °C, microporous AC showed over 4-fold increase in capacity.
- Most S-AC cathodes showed favorable performance in a 3 M electrolyte at 70 °C.
- Increasing molarity from 3 M to 5 M reduced capacity in microporous S-AC.
- Molarity increase had little effect on the capacity of mesoporous S-AC samples.

ARTICLE INFO

Article history:
Received 9 July 2013
Received in revised form
9 September 2013
Accepted 1 October 2013
Available online 11 October 2013

Keywords:
Li–S
Activated carbon
Pore properties
Polysulfide
Dissolution

ABSTRACT

In this paper, we adopted three different commercial activated carbon samples (ACs) having different particle size, specific surface area and pore size to make sulfur–carbon (S-AC) nanocomposites for rechargeable lithium sulfur batteries. The effect of the physical parameters of ACs and the combined effect of electrolyte molarity were investigated. The performance of the cells at two different temperatures of 25 and 70 °C were compared. For room temperature operation of the cells, the capacities of S infiltrated into microporous AC having smaller pore size and stronger interactions with sulfur and sulfides were lower than those of the S infiltrated into micro- and mesoporous ACs containing larger pores. In contrast, the microporous AC demonstrated higher capacity at the elevated temperature due to the improved ion transport rate. The effect of electrolyte molarity on the performance of Li/S cells was found to depend on the AC pore size and particle size distributions. Increasing electrolyte molarity from 1 to 3 M demonstrated improved cell performance and reduced polysulfide dissolution in all the studied S-AC samples. However, further increasing electrolyte salt concentration resulted in a high polarization and reduced cell performance in S-ACs having large particle size or smaller pores.

1. Introduction

Lithium-ion (Li-ion) batteries have become one of the most advanced electrical energy storage technologies widely used in our life in various portable applications, such as smart phones, laptop computers and tablets, cameras and other portable electronic devices. However, the performance of current Li-ion batteries does not fulfill the increasing demands of complex portable devices, household supplies, and transportation system [1–3]. Consequently, new materials and new chemistries need to be explored in order to achieve higher energy densities of Li-ion batteries. Among several candidates, sulfur (S) is an attractive cathode material due to its high theoretical gravimetric capacity (1672 mAh g^{-1}), low cost, and environment friendliness. These advantages motivated many researchers to consider S in various battery systems such as Na/S, Al/S, Li/S, etc. [4–7]. Li/S system has received the greatest attention because it offers a potential for a very high energy density with the theoretical specific energy and volumetric energy density of 2600 Wh kg^{-1} and 2800 Wh L^{-1}, respectively, which are much higher than theoretical energy storage characteristics of commercial Li-ion cells (~600 Wh kg^{-1} and ~2000 Wh L^{-1}) [3,8].

Despite of the advantages of S, several challenges need to be overcome for the successful commercialization of Li/S chemistry: a poor stability of S-based cathodes and their high resistance and thus low power characteristics. The intermediate discharge products, high-order polysulfides (such as Li_2S_8 or Li_2S_4), can be dissolved in electrolytes, resulting in a reduced S utilization and polysulfide shuttle phenomenon. The "polysulfide shuttle" refers to

* Corresponding author.
E-mail address: yushin@gatech.edu (G. Yushin).

0378-7753/$ – see front matter © 2013 Elsevier B.V. All rights reserved.
http://dx.doi.org/10.1016/j.jpowsour.2013.10.003

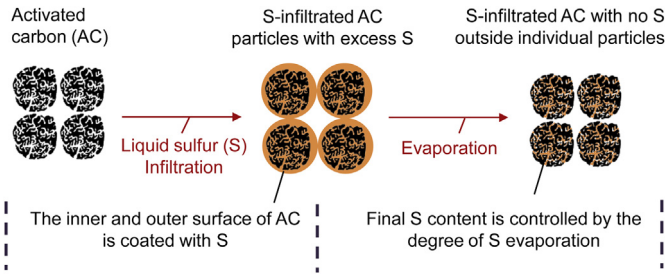

Fig. 1. Schematic of S-AC composite powder fabrication.

the diffusion of polysulfides alternating between Li anode and S cathode based on the concentration gradient [8,9]. This also causes random deposition of the final discharge product, electrically insulative and insoluble Li_2S_2 and/or Li_2S onto the surface of both electrodes, blocking the electrolyte access and thus lowering the active mass utilization [10,11]. Moreover, intrinsic low electronic conductivity of S, Li_2S_2 and Li_2S requires efficient conductive matrix for high capacity and rate-capability.

The challenges described above can, in principle, be overcome by several approaches. One approach is to develop electrolytes or electrolyte additives, which would greatly reduce the solubility of the polysulfides. Ionic-liquid based electrolytes or solid electrolytes were found to repress the shuttle mechanism [12–15]. High concentration of LiTFSI salt [16–18] in commonly used electrolyte solvents was found to significantly reduce the polysulfide solubility at the expense of a lower ionic conductivity and higher viscosity of these electrolytes. The addition of Li_2S_8 into electrolyte [19] or the optimized composition of ternary electrolyte system [20] have been also shown to alleviate the dissolution of S cathodes. The use of $LiNO_3$ or Li_2S/P_2S_5 additives in an organic electrolyte was found to induce a more stable solid electrolyte interphase (SEI) layer on Li electrodes, which similarly minimizes the shuttle mechanism and stabilizes cell resistance [21,22].

A complementary approach is embedding S into conductive matrix such as carbon and conductive polymer including activated carbon (AC), carbide derived carbon (CDC), carbon nanotube (CNT), graphene, polyaniline [18,23–29] to enhance electronic conductivity of the S-based cathodes and, at the same time, to reduce the S dissolution via its interaction with carbon and confinement in carbon pores. When S is entrapped inside of a carbon matrix, a characteristic diffusion time for polysulfides required for their transport into the bulk electrolyte becomes longer (in an ideal case – significantly longer than a typical charge–discharge time). This approach is also advantageous for improving the utilization of S, because non-conductive S is in contact with the electrically conductive media [11,23,26,30–36].

While promising performance of many S-containing carbon nanocomposites have been reported [11,18,23,26,30–36], surprisingly limited understanding exists on the effects of physical structural parameters of porous carbon on the electrochemical performance of Li/S–C cells. Since the rate of the capacity degradation is greatly affected by polysulfide dissolution and pore blocking by the re-deposition of Li_2S on the electrode surface, the cell performance could be affected by both the structural properties of porous carbons and the properties of electrolyte. Furthermore, it

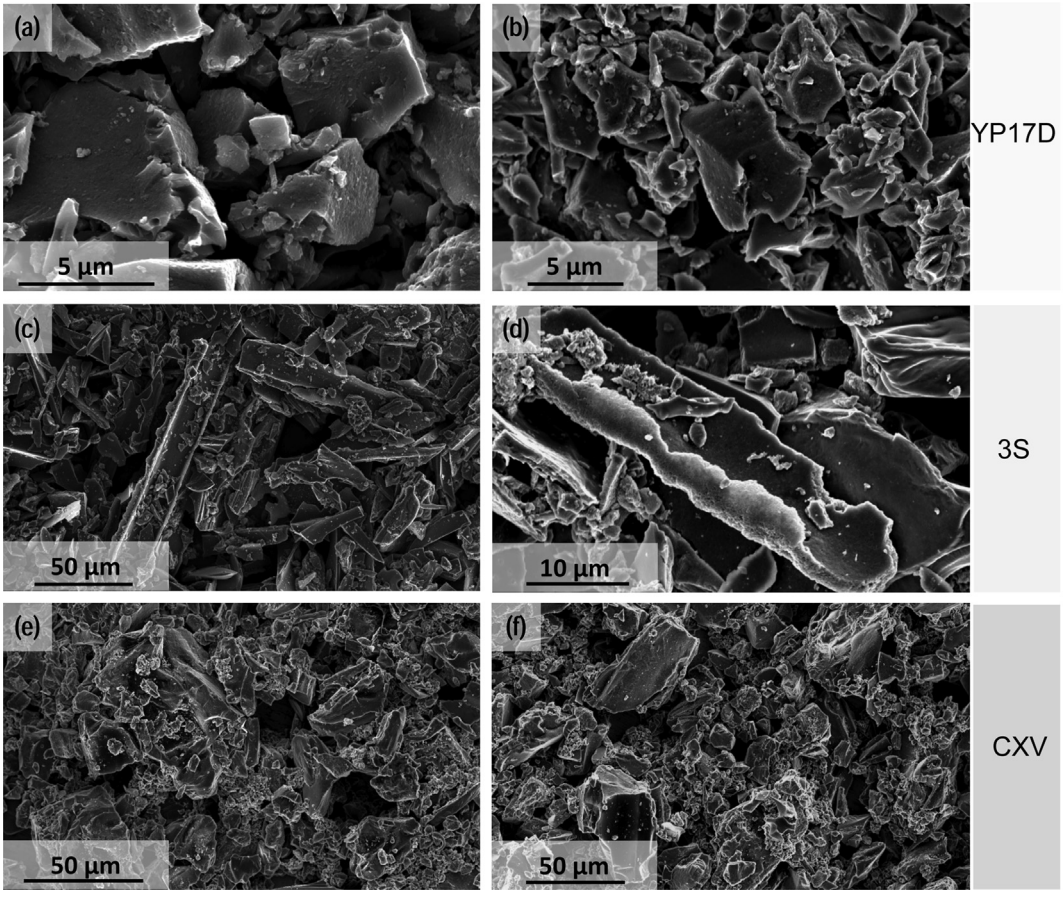

Fig. 2. SEM micrographs of AC and S-AC composite powders; (a) YP17D, (b) S-YP17D, (c) 3S, (d) S-3S, (e) CXV, and (f) S-CXV.

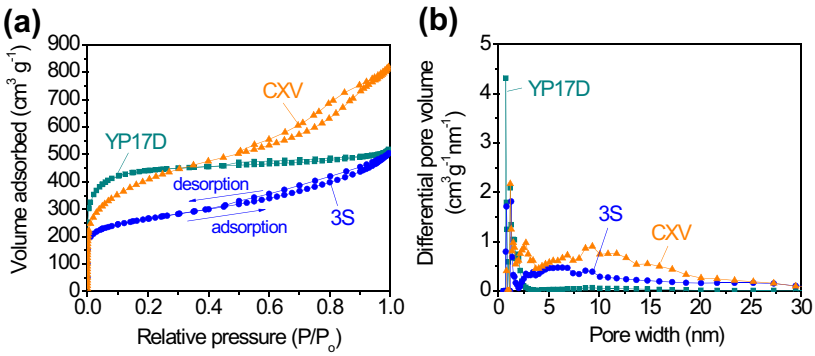

(c)	BET SSA (m^2/g)	Pore Volume (cc/g)	Pore Size Distribution
YP17D	1586	0.80	0.7-2.5 nm
3S	971	0.78	0.7-30 nm
CXV	1488	1.27	0.8-30 nm

Fig. 3. Porosity characterization of commercial AC samples used in our study: (a) N_2 sorption isotherms, (b) pore size distribution, (c) key pore characteristics.

may be expected that the complex electrode/electrolyte interactions could be affected by temperature.

In this study, we aimed to reveal the impacts of the pore size distribution, pore volume and specific surface area of porous carbons on the temperature-dependent electrochemical performance of S-infiltrated carbon cathodes in electrolytes having different salt concentrations. While many advanced porous carbon synthesis techniques have been developed in the last decade [37–40], we believe that AC will likely remain the material of choice for use in the majority of commercial applications due to their scalable and reliable production [3,41–43]. In order to make this study most relevant to industrial needs, we used low-cost commercial AC samples produced from natural precursors and having markedly different porosity characteristics for S–C composite fabrication and evaluation.

2. Experimental

Three AC samples have been used: Ceca 3S and CXV (Arkema Group, France) and YP17D (Kuraray Chemicals, Japan). The S (Alfa Aesar) melted at 120 °C was first infiltrated into AC pores. After this step the AC pore surface was entirely coated by S. In order to

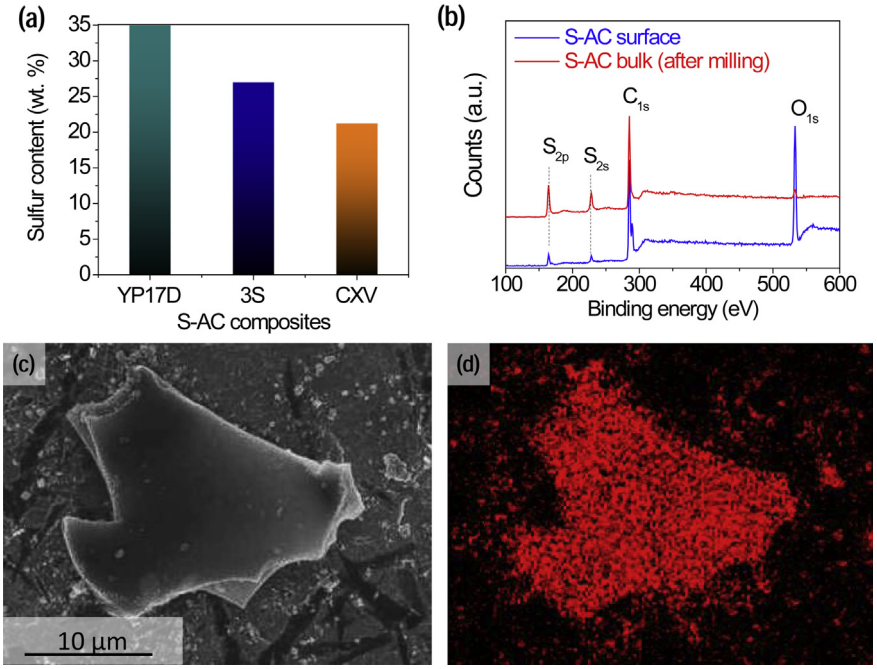

Fig. 4. S-AC characterization: (a) S fraction in S-AC composites as measured using a TGA, (b) XPS spectra of a representative S-AC electrode before and after ion milling, (c) an SEM micrograph of a single representative S-AC particle, and (d) EDS mapping of the S distribution within this particle.

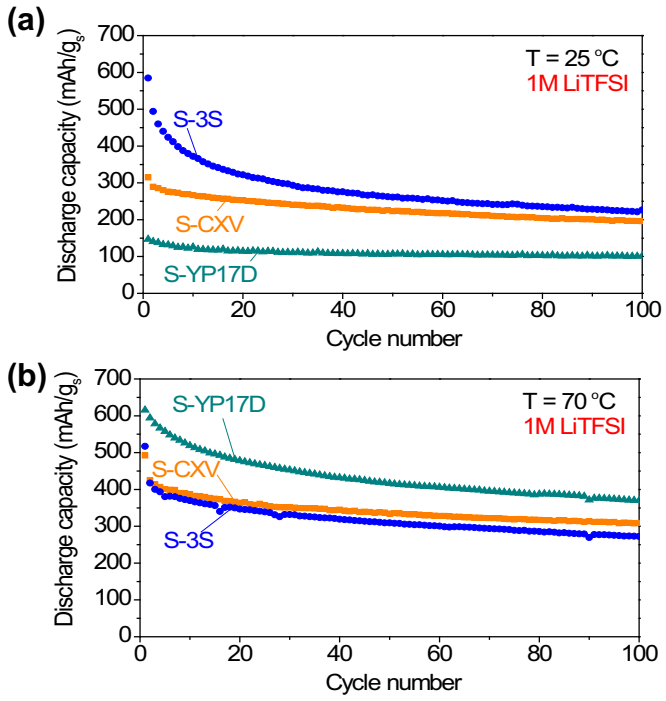

Fig. 5. The cycle stability of different S-AC cathodes with 1 M Li salt at C/5 at (a) 25 °C and (b) 70 °C. The capacity is normalized by the weight of S.

provide a pore volume needed for ~80% expansion during S lithiation with the Li_2S formation and in order to remove excess of S from the exterior surface of AC particles, the S-infiltrated AC samples (S-AC) have been thermally treated at 220 °C for 2 h, as described in Fig. 1.

To prepare uniform slurry for electrode casting, the S-AC powders were mixed with a polyacrylic acid (PAA) (Sigma Aldrich, USA) binder dissolved in ethanol. We have previously showed that PAA with uniformly distributed polar functional groups serve as an excellent binder for anodes and cathodes [44,45]. Similar to our previous studies, the ratio of active material (S-AC) to PAA binder was 85:15 and no conductive additives were used. The slurry was stirred at room temperature for 30 min and casted on a nickel (Ni) foil current collector. After drying the electrode overnight under vacuum, coin cells were assembled with the electrolytes composed of 1 M, 3 M, and 5 M bis(trifluoromethanesulfonyl)imide (LiTFSI) salt in dimethoxyethane (DME):1,3-dioxane (DIOX) (1:1, v:v) solvent, celgard 2325 (Celgard) separator and pure Li foil [Alfa Aesar, 99.9%] anode. 0.2 M $LiNO_3$ [Alfa Aesar, 99.99%] was added to the electrolyte as an additive. The cells were equilibrated for 24 h before operation. The S loading in the electrode was kept at ~0.5 mg cm^{-2}.

The coin-cells assembled inside an Ar glove box (<1 ppm of H_2O, Innovative Technologies) were cycled between 3.0 V and 1.2 V vs. Li/Li$^+$ (V) in a galvanostatic mode by using an Arbin battery testing system (Arbin Instruments, USA). The cells were tested with different C-rates at C/20, C/10, C/5, C/2, 1C, C/20 and then the durability test was continued at C/5 for 200 cycles. C-rates were calculated based on the theoretical capacity of S and the S mass in each electrode.

Zeiss Ultra60 FE-SEM (Carl Zeiss, Germany) was used to perform scanning electron microscopy (SEM) and energy dispersive X-ray spectroscopy (EDS) studies at a beam voltage of 5 kV and a working distance of 4 mm for imaging and 8 mm for EDS, respectively. After cycling test, the coin cells were disassembled and both anodes and cathodes were washed with dimethyl carbonate (DMC) to remove residual salts in the glove box atmosphere. The SEM samples were transferred from a glove box to a sealed plastic bag, limiting air exposure to time under <5 min. X-ray photoelectron spectroscopy (XPS) analysis was done by using the Thermo K-Alpha (Thermo Scientific, USA) (Al K_α peak) with a step size of 1 eV for the survey scans to confirm elemental composition of both the electrode surface and the bulk. The X-ray gun produced a 200 μm spot size, and an electron flood gun was used for charging compensation. Ion milling was performed within the XPS in order to gain the S composition with the bulk of the electrode. This milling was carried out by rastering an Ar^+ ion beam operated at 3 kV for 10 min. Thermogravimetric analysis (TGA) was performed from room temperature to 600 °C under nitrogen (N_2) atmosphere at a heating rate of 5 °C min^{-1} using a TGA Q50 analyzer (TA instruments, USA) to calculate S content in S–C composite. The isotherms of N_2 gas adsorption on the surface of ACs were collected at 77 K using an ASAP 2020 surface area and porosity measurement system (Micromeritics Inc., USA). Monte Carlo simulation of electron trajectory for EDS analysis was done with a CASINO software. Due to the complex nature of porous material, we simplified our composite material to solid material with hypothetical density which is the mixture of density of S (2.07 g cm^{-3}) [46], amorphous C (2.0 g cm^{-3}) [47], and unoccupied pore (0 g cm^{-3}) as follows. $\rho_{eff} = (m_C + m_S + m_p)/(V_C + V_S + V_p)$ where ρ_{eff} is effective density, m_C is carbon mass fraction, m_S is sulfur mass fraction, m_p is pore mass fraction, V_C is carbon volume fraction, V_S is sulfur volume fraction, and V_p is pore volume fraction. The calculated effective densities were ~0.87, ~0.86, and 1.02 g cm^{-3} for S-YP17D, S-3S, S-CXV AC samples respectively.

3. Result and discussion

The morphologies of AC and S-AC cathode powders are typical for commercial ACs produced from natural precursors – irregular shapes and a broad particle size distribution (Fig. 2). YP17D has the smallest particle size (around 1–5 μm). The 3S samples exhibit elongated shape with high aspect ratio and particle size up to ~3 μm in the smallest dimension and up to ~150 μm in the largest dimensions. The CXV also shows large particle size in the range of 10–50 μm.

Fig. 3a exhibits N_2 sorption isotherm of ACs. YP17D shows the type I shape of the isotherm according to the Brunauer classification with saturation at relative pressure (P/P_0) of 0.2 which indicates pores are mainly microporous (≤2 nm) with small volume of pores larger than 2 nm. In contrast, 3S and CXV demonstrate type IV isotherm suggesting presence of both micropore and mesopores (pores with size in the 2–50 nm range). The adsorption–desorption hysteresis of CXV is larger than the same of 3S and this suggests that CXV possesses larger volume of mesopores. These conclusions are fully supported by the pore size distribution (PSD) curves obtained from the N_2 isotherms based on density functional theory (DFT) calculation (Fig. 3b). We assume that the shape of the pores can be approximated as a slit, which is a common assumption for ACs [48]. The porosity data including BET surface area, pore volume, and pore size distribution for all AC samples are summarized in Fig. 3c. YP17D and CXV have comparable BET surface area and pore volume, but the great difference is that the CXV includes larger pore size up to 30 nm. 3S has smallest surface area and pore volume, and the particle and pore size distribution are similar to CXV.

After infiltration of the melted S into AC, the S excess was evaporated at a fixed temperature of 220 °C. We can observe that our procedure of S evaporation (Fig. 1) allowed us to completely eliminate S presence outside the particles or on their surface

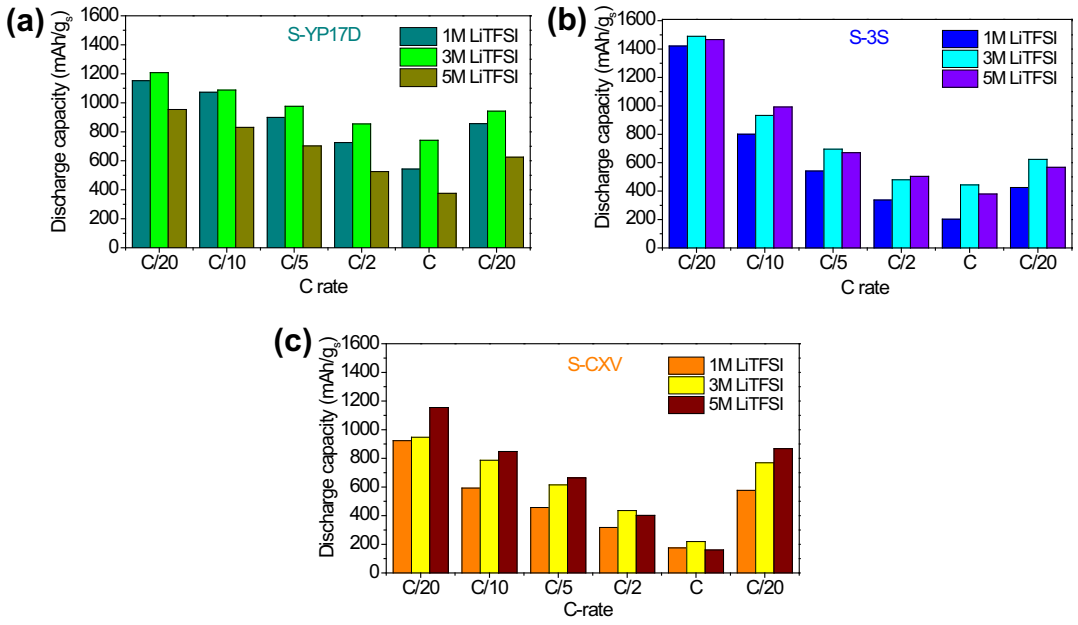

Fig. 6. Rate performance of S-AC composites in different electrolyte molarities: (a) S-YP17D, (b) S–3S, and (c) S-CXV. The tests have been carried out at 70 °C and the capacity is normalized by the weight of S. The cells were tested at C/20, C/10, C/5, C/2, and 1C consecutively and once again at C/20 to reveal the degree of degradation.

(Fig. 2b, d, f), which is critically important for our studies. Since the structural properties, surface area and pore size of the ACs were different, each AC expectedly retained different S capacity as shown in Fig. 4a. YP17D contains the largest amount of S (~35%) due to the high specific surface area and, equally important, the smallest pores present. Smaller pore size results in a stronger integration between S and C because the interaction potentials between the S molecules (mostly S_8) and both sides of the pore walls overlap. As a result, they entrap larger S content in the pores. While CXV has larger pore volume and similar specific surface area compared to YP17D, it entraps less S into its pores (~21%) due to larger pore size. 3S has similar pore volume but smaller specific surface area compared to YP17D. Again, due to the presence of large pores, 3S entrapped smaller S content than YP17D however the mesopore volume of 3S is smaller than CXV hence it can store larger amount of S than CXV. The S loading capacity of ACs evidently depends more on the pore size than on the overall pore volume and surface area. XPS depth profiling analysis was carried out to qualitatively reveal possible changes in S content on the surface of the S-AC particles. Indeed, we found that the intensity of C_{1s} peak decreases significantly with milling depth, while those of the S_{2s} and S_{2p} peaks increases. Fig. 4b shows an example of the survey XPS spectra collected before and after 10 min milling, demonstrating higher S content after removal of the surface (S/C weight ratio changed from 0.13 to 0.60). The accurate estimation of etched thickness is challenging because ACs have random structure and there is no such standard material. However it was reported that our XPS machine has a ~15 nm min^{-1} etch rate of SiO_2 under same experimental condition [49]. The uniformity of S infiltration within the porous C network was confirmed using EDS line scans and EDS mapping across individual particles. Fig. 4c, d shows an example of such results, demonstrating uniform distribution of S within a ~10 μm S-CXV particle.

It has been previously reported that the bimodal porous carbon materials possess certain benefits as a matrix for S–C composite cathodes, because they generally can provide large pore volume for S infiltration, mesopores for rapid ion transport and thus high power performance and small pores for reduced polysulfide dissolution [18,50]. The micropores additionally often provide higher surface area available for good electrical contact with S, which enhances the S utilization. Similar arguments could be used to explain a significant difference in the performance of the selected ACs. While microporous S-YP17D cathode with slow ion transport (with some of the pores being likely blocked by S) shows very low capacity utilization at room temperature, mesoporous S-3S and S-CXV exhibit significantly higher capacities (Fig. 5a). The S-3S electrode with the large pores shows the highest initial capacity, however, it suffers from the fastest fading due to the low surface area and large pores, which should reduce their polysulfides' confinement properties (Fig. 5a). For elevated temperature operation (70 °C) when ion diffusion within the S–C composites is significantly enhanced, the situation changes dramatically with S-YP17D (exhibiting the highest surface area of carbon) now showing the highest specific capacity over the other two S-AC cathodes

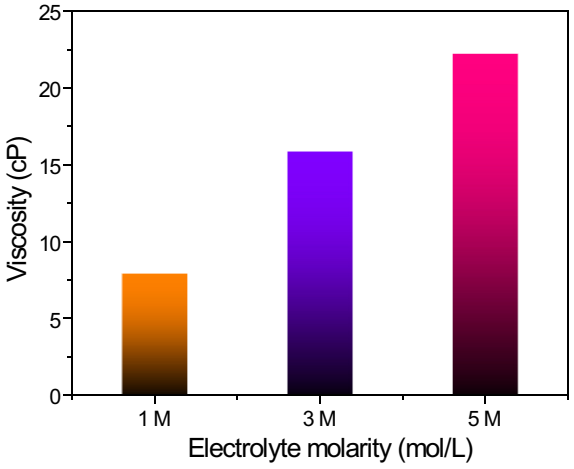

Fig. 7. The viscosity of electrolytes with different LiTFSI salt concentration in a DME:DIOX (1:1) solvent mixture at room temperature.

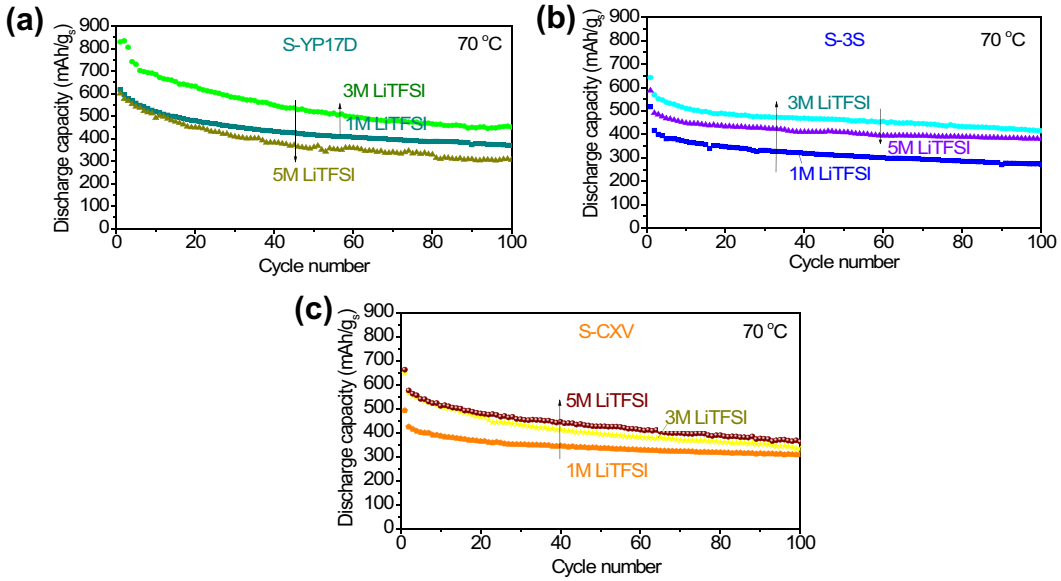

Fig. 8. The comparison of cycle stability of different S-AC cathodes with different electrolyte molarities: (a) S-YP17D, (b) S-3S, and (c) S-CXV. The tests have been carried out at 70 °C and the capacity is normalized by the weight of S.

(Fig. 5b). All the cells with 1 M LiTFSI salt were compared to investigate temperature effect. In our previous studies we observed conformal coating of the re-deposited lithium sulfide on the particles' surface [28]. The blocking of small micropores (as in YP17D) by the agglomerated re-deposited lithium polysulfides can be reduced at elevated temperatures, so the benefits of high temperature are more visible with this microporous carbon. Moreover, the lower viscosity of electrolyte at high temperatures helps electrolytes to reach even in micropores in S–C composites, improving the S utilization dramatically. Note that the mesoporous S-3S, having

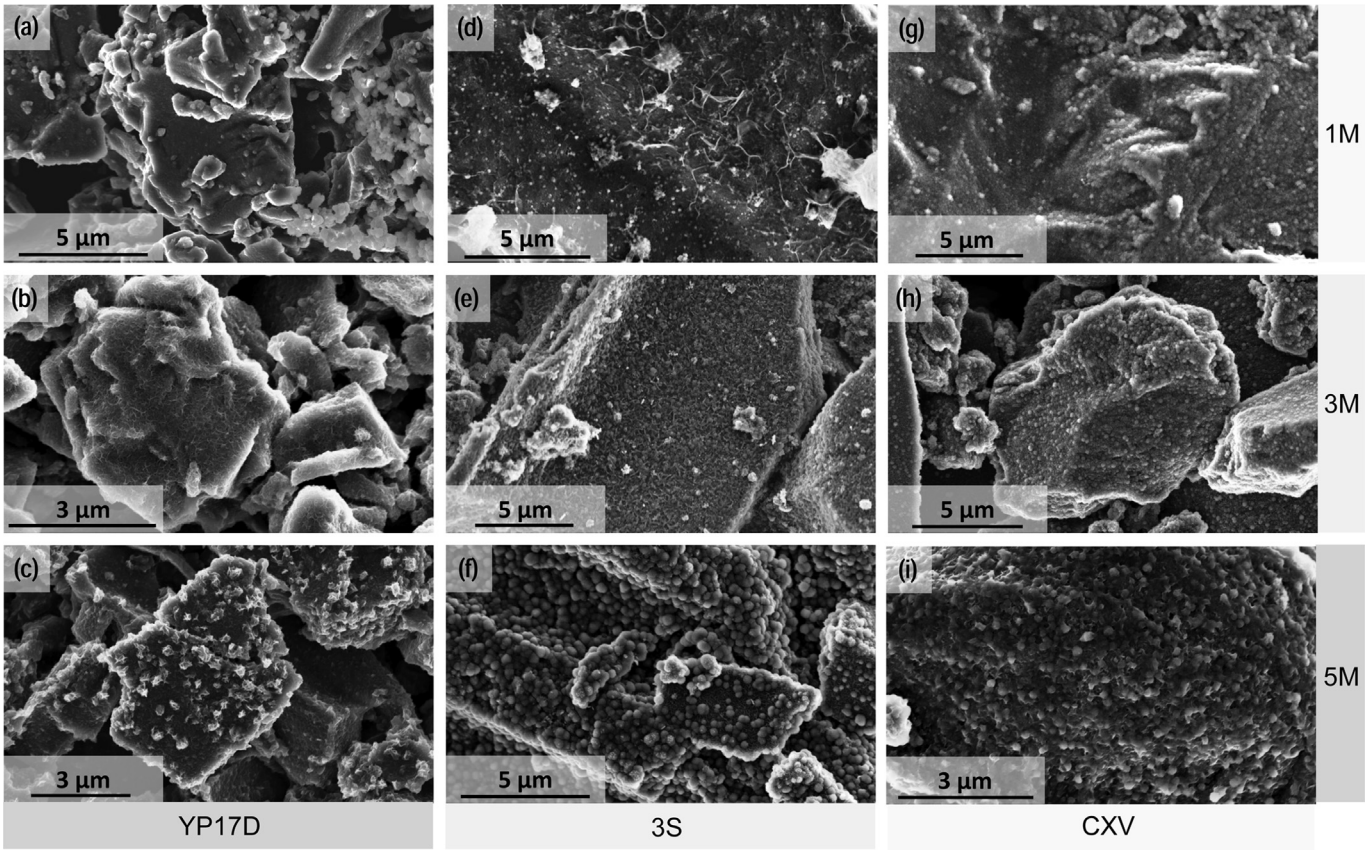

Fig. 9. SEM micrographs of cathodes cycled at 70 °C in electrolytes having different molarity (salt concentrations): (a) S-YP17D-1 M, (b) S-YP17D-3 M, (c) S-YP17D-5 M, (d) S-3S-1 M, (e) S-3S-3 M, (f) S-3S-5 M, (g) S-CXV-1 M, (h) S-CXV-3 M, (i) S-CXV-5 M.

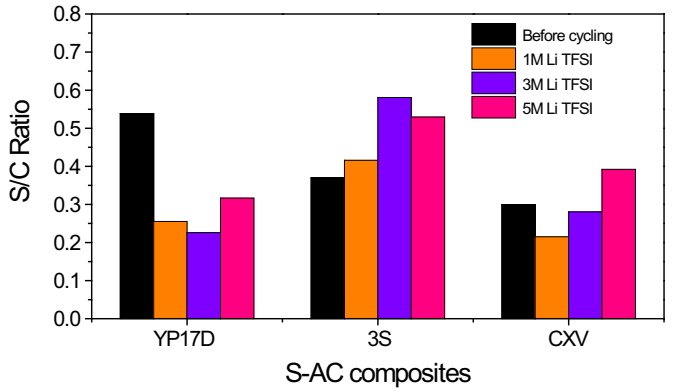

Fig. 10. EDS chemical composition of the SAC electrodes after cycling at C/5 at 70 °C.

the smallest surface area and the large pores, exhibits virtually identical performance at both temperatures (compare Fig. 5a and b). This suggests that the ion diffusion was sufficiently fast at room temperature.

The C-rate performances of the three samples with different Li salt concentration in electrolytes are compared in Fig. 6. Because a series of charge–discharge tests with increasing current density were performed on the same cell, the rate test actually corresponds to the combined effect of both the stability of the cathodes (polysulfide dissolution) and its S utilization with increasing current density (rate-capability). Therefore in order to reveal the degree of cell degradation, at the end of this test we have performed a second slow (C/20) charge–discharge test. S-YP17D shows the highest rate performance at 70 °C, which is rather surprising due to its smallest pore size. Furthermore, its good rate capability was observed in electrolytes having various salt concentrations.

More specifically, at a slow rate of C/20 S-YP17D shows the discharge capacity of 834–1270 mAh g_s^{-1} (up to 76% S utilization), which reduces to 375–742 mAh g_s^{-1} (up to 44% S utilization) at 1C, which corresponds to ~59% capacity retention. However, taking into account the electrode degradation and comparing the "1C" performance to the next cycle collected at "C/20" we can estimate the capacity retention of up to 79% when increasing the current density by 20 times, which is quite high considering the small pore size and large particle size of this sample. Such good rate performance of S-YP17D can be explained by its bottle-neck free pores (this type of AC has been optimized for use in high-rate electrochemical capacitors). In case of S-3S composite sample, it shows the highest initial sulfur utilization of 1400 mAh g_s^{-1} (83% utilization, likely due S being very accessible to electrolyte), but it quickly loses its capacity with cycling (compare "C/20" performance before and after rate tests, Fig. 6b). By comparing the "1C" performance to the next cycle collected at "C/20" we estimate the capacity retention of up to 67% when increasing the current density. Reduced (compared to microporous S-YP17D sample) rate performance of this sample could be related to its slightly larger particle size and possibly more tortuous pores. The pore tortuosity, unfortunately, is difficult to characterize. S-CXV shows the worst rate performance of all the samples, where its capacity at "1C" is only 19–30% (depending on electrolyte) of that at "C/20" even when considering fading rate. We propose that its largest particle size is responsible for the poor rate performance (diffusion time is proportional to the square of diffusion distance and CXV particles are almost 10 times larger than YP17D). When considering the fading rates among these AC samples, it is evident that the mesopores facilitate the polysulfide dissolution. Both the large particle size and large surface area of S-CXV may assist this sample to reduce its polysulfide dissolution and the resulting fading rate in spite of having a significant mesopore volume.

In all ACs, 3 M electrolyte showed superior performance compared to 1 M electrolyte due to the reduced polysulfide dissolution based on the common ion effect and smaller fraction of solvent molecules not bound to the electrolyte ions and available for such a dissolution [16,17]. Further increasing Li salt concentration reduced the performance of microporous S-YP17D electrode, likely due to its higher viscosity (Fig. 7) and thus possibly reduced electrolyte mobility in small micropores. Because of this high viscosity of 5 M electrolyte, not all S–C composite cathodes may benefit from its properties. For example, the study of Shin et al. [16],

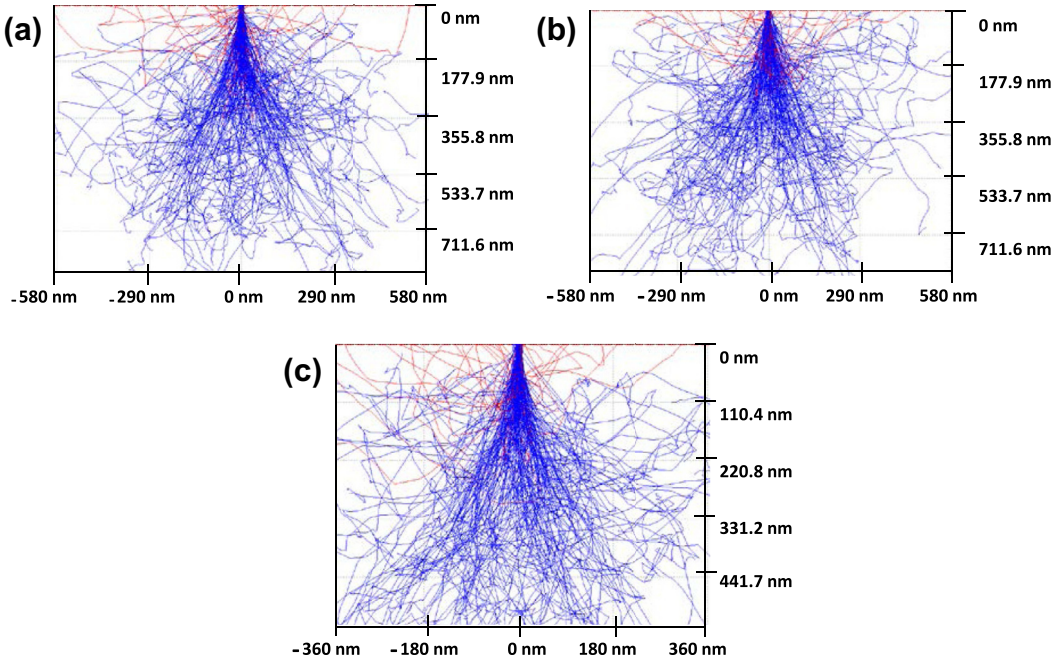

Fig. 11. Monte Carlo electron trajectory simulation, revealing the sample depth, from which EDS signal is collected: (a) S-YP17D, (b)S–3S, and (c) S-CXV.

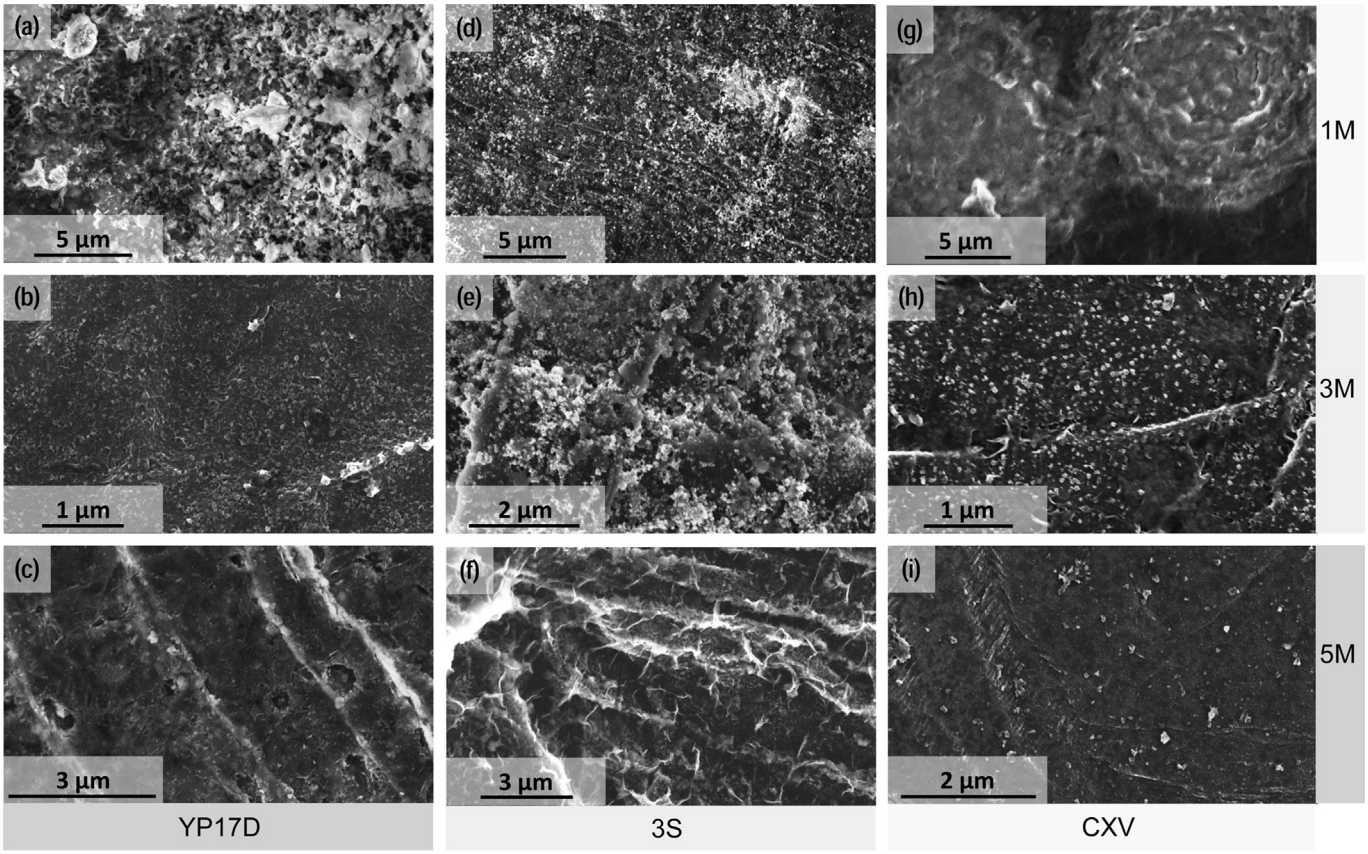

Fig. 12. SEM micrographs of Li anode surfaces after cycling at 70 °C against different S-AC composite cathodes in electrolytes having different salt concentration: (a) S-YP17D-1 M, (b) S-YP17D-3 M, (c) SYP17D-5 M, (d) S-3S-1 M, (e) S-3S-3 M, (f) S-3S-5 M, (g) S-CXV-1 M, (h) S-CXV-3 M, (i) S-CXV-5 M.

Suo et al. [17] and Lee et al. [18] suggested that increase in Li salt concentration to 5–7 M level significantly reduces and eventually prevents polysulfide dissolution and improves cell stability. In contrast, Mikhaylik et al. utilized graphite as a carbon source and reported that small amount Li salt increase (0.5–0.85, and 2.5 M LiTFSI in DME/DIOX) showed inferior performance with reduced S utilization [51]. Our current results similarly suggest that optimal Li salt concentration depends on the physical properties of carbon.

Long-term cycling performance of three types of S-AC cathodes with increased Li salt concentration at "C/5" rate is shown in Fig. 8. Overall, the initial capacities in the range of 400–800 mAh g_s^{-1} gradually decreased to 300–500 mAh g_s^{-1} after 100 cycles. The S-YP17D cathode showed the highest initial capacity, but similar to other sample, relatively fast capacity reduction. The small micropores of this sample must be easily blocked by the reaction products, Li_2S and Li_2S_2. Only the S-CXV sample, having the largest pore size, exhibited the best performance in most viscous, 5 M, electrolyte.

Because the long term cyclability is greatly affected by the low order polysulfide precipitation on the cathodes (blocking the electrolyte pathway and lowering the S utilization) [16], the surface of cycled S-AC cathodes were investigated with SEM and EDS. The SEM images in Fig. 9 show all ACs have similar outcomes in terms of higher polysulfide precipitation with increasing electrolyte salt concentration and electrolyte viscosity.

The S-YP17D in 1 M electrolyte showed relatively clean surface but, the remaining S content detected by EDS (Fig. 10) was noticeably lower than the initial value, indicating that a large portion of S was dissolved in spite of the polysulfide confinement in the micropores of YP17D. These results are consistent with the capacity fading observed in charge–discharge tests. What appeared surprising, though, mesoporous S-CXV and S–3S showed higher S content after cycling and such S content generally was higher in electrodes cycled in electrolytes with higher molarity. On one hand, since these electrodes had larger content of "inactive" S (Fig. 8) and a similar degree of electrochemical degradation (Fig. 10), it could make sense that more S would stay in such samples after cycling. The puzzle was where these extra S came from. Simulation results of the penetration depth of electrons (~600–800 nm) in our ACs at the employed accelerating voltage explained the observed phenomena – the majority of the EDS signal comes from the top 500 nm layer on the particles' surface, being far smaller than the particles' diameter (Figs. 2 and 9). This top layer is covered by the precipitated polysulfides (Fig. 9), therefore showing lower C and higher S content by the EDS.

Building a protective, electrically insulative SEI layer on a Li anode surface may improve stability of Li/S cells [28]. The surfaces of the cycled Li anodes showed significant differences in their morphology and composition (Fig. 11). While the Li surface cycled in 1 M electrolyte shows relatively rough surface with more dendritic structures, higher salt concentration resulted in a significantly smoother and more flat surface. During cycling, there is a reaction competition on the surface of Li between forming a stable SEI with the electrolyte and reacting with diffused polysulfides. High molarity electrolyte can provide more stable SEI formation because of the reduced polysulfide diffusion. Our results are in agreement with previous studies showing that high salt concentration can develop thicker SEI on a Li electrode [17], hence mitigating undesired side reactions between polysulfides and a Li metal (Fig. 12).

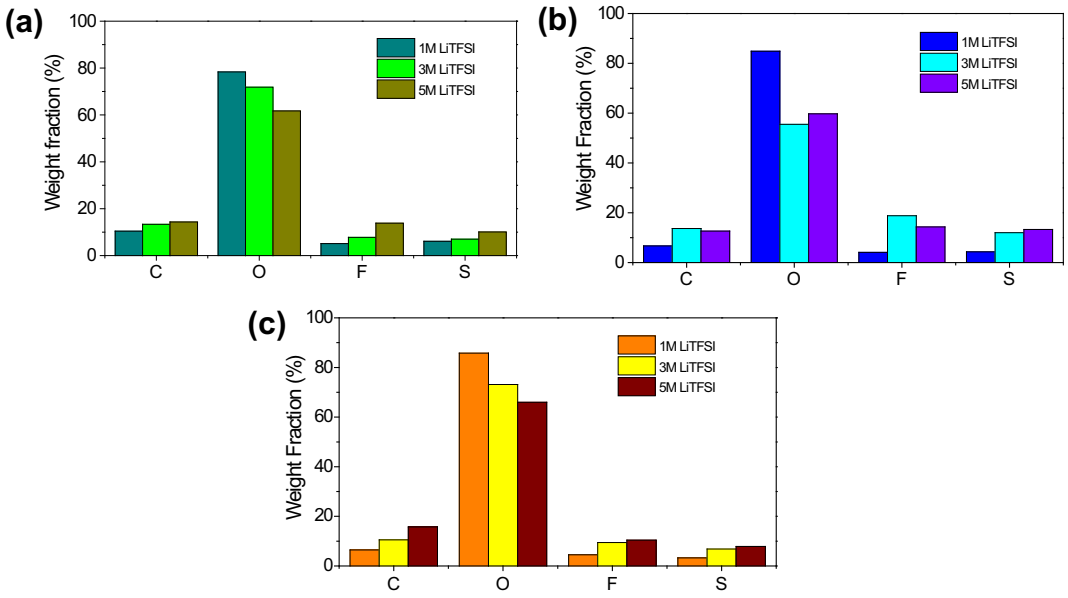

Fig. 13. EDS chemical analyses of the Li anodes after cycling at 70 °C against different cathodes: (a)S-YP17D, (b)S-3S, and (c) S-CXV.

EDS on the cycled Li anodes confirmed the presence of C, O, F, and S, which are the typical components of SEI on a Li anode in Li/S cells (Fig. 13). Possible SEI products are $Li_2S_2O_4$, Li_xSO_y, LiS, Li_2S, LiF, $LiCF_3$ and organic species were produced by Li salt and solvent decomposition [21]. Generally, the C, F, and S increases with the salt concentration, but the oxygen content shows opposite trend. We believe that the oxygen is mostly come from the unintentional oxidation of the samples in air while transferring to an SEM

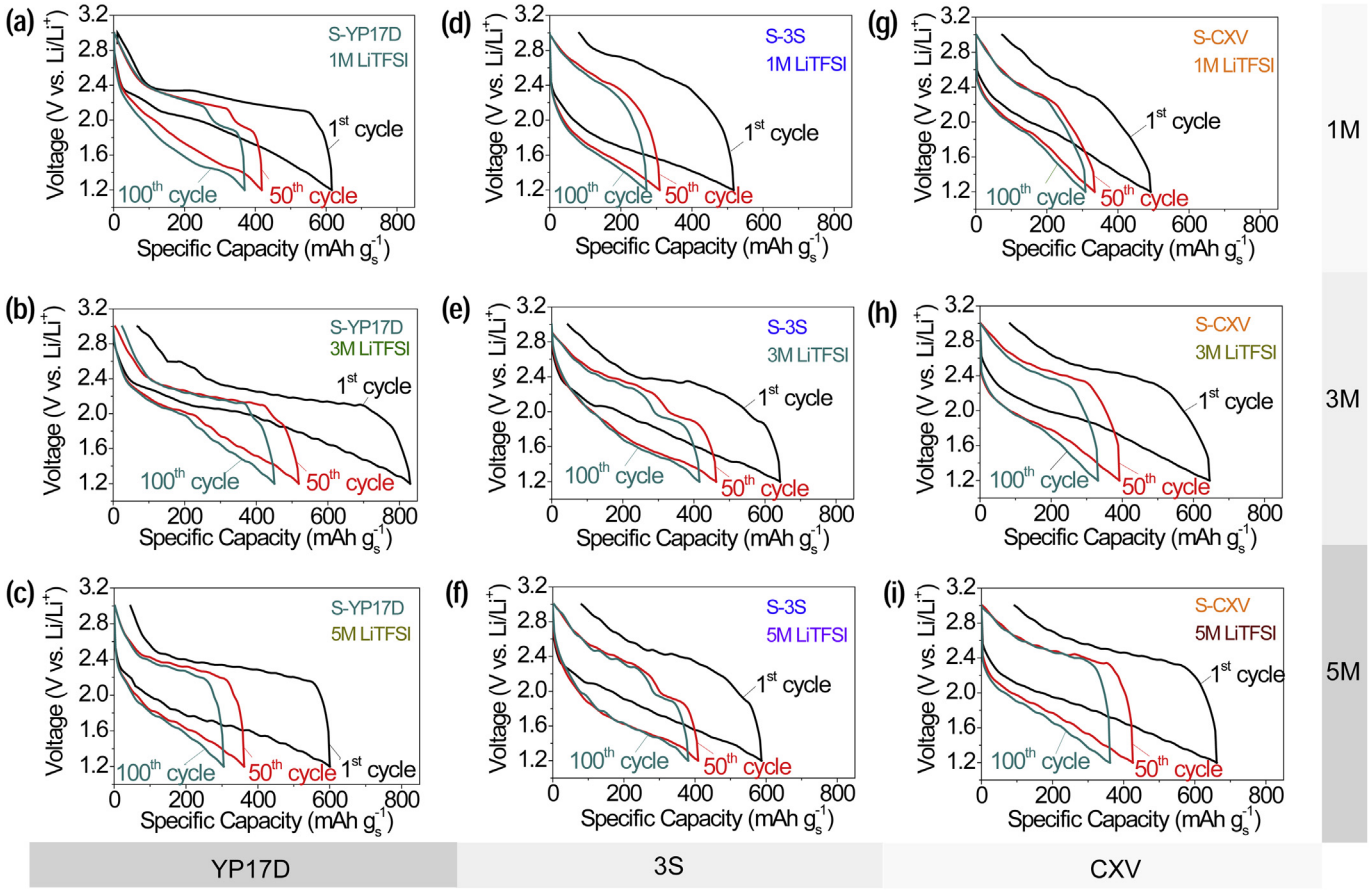

Fig. 14. The voltage profiles of S-AC composite cathodes in electrolytes having different salt concentration at the 1st, 50th and 100th charge–discharge cycles recorded at C/5 rate at 70 °C: (a) S-YP17D-1 M, (b) SYP17D-3 M, (c) S-YP17D-5 M, (d) S-3S-1 M, (e) S-3S-3 M, (f) S-3S-5 M, (g) S-CXV-1 M, (h) S-CXV-3 M, (i) SCXV-5 M.

chamber. The lower O content with higher other SEI components in high salt concentration supports the thicker SEI layer formation, which can protect the Li and SEI from being oxidized during the air exposure [17].

Fig. 14 shows the voltage profiles of the S-AC cathodes during cycling at 70 °C. It is well known that S discharge curve commonly shows two plateaus at ~2.4 V and ~2.0 V in DME/DIOX [10]. Such plateaus, however, could only be seen in an S-YP17D sample. Both 3S and CXV show relatively featureless curves with a large polarization and resulting voltage hysteresis from the very first cycle. Large particle size and rapid S dissolution during the 1st cycle in these two electrodes may contribute to the observed phenomena. Effect of the electrolyte concentration could be mostly seen in S-YP17D and S-CXV, which showed larger polarization in a 5 M electrolyte, likely due to reduced ionic mobility in the smaller pore present in such samples. With increasing cycle number, all the cells show significantly increased polarization and lower capacities, likely resulting from the electrically and ionically insulative precipitations of the lithium sulfides on both the Li anode and S-AC cathodes.

4. Summary

In this study, three different ACs (YP17D, 3S and CXV) having different particle size, specific surface area and pore size were used as S hosting materials. Uniform S infiltration was achieved in all samples, including those having large (up to 50 μm) particle size. Under identical S infiltration/evaporation conditions, microporous AC (YP17D) retained the highest S content. The effect of the physical parameters of ACs and the combined effect of Li salt concentration were investigated to provide guidelines for the optimization of electrode/electrolyte systems in Li/S batteries. The performance of the cells at two different temperatures of 25 and 70 °C were compared.

The pore size and particle size distribution of the AC were found to have a significant impact on the accessible specific capacity of S in electrolytes having different molarities. The most significant difference was observed at room temperature, where strictly microporous S-YP17D exhibited very small capacity, in contrast to mesoporous S-ACs. Room temperature tests also revealed better capacity retention and smaller capacity in S-ACs having larger particle size. At an elevated temperature of 70 °C (higher ionic mobility) microporous S-YP17D with smallest particle size showed over 4-fold increase in capacity. However, the capacities of S-ACs with mesopores and large particles (S-3S and S-CXV) were not affected by temperature or increased only slightly at higher temperatures, suggesting that either an electron transport is a rate-limiting step in the corresponding reduction–oxidation reactions of these cathodes or the increased ionic transport is significantly offset by the increased cathode dissolution. The cathode dissolution rate within the few initial cycles at 70 °C was the highest in mesoporous S-ACs having the smallest specific surface area (S-3S). Quite remarkably, the best rate capability at 70 °C was observed in microporous S-YP17D, suggesting that at this temperatures the rate may be limited not by the diffusion of ions within the pores, but rather by the diffusion of ions through the polysulfides deposited on a Li foil and re-deposited on the surface of S-AC particles. Increasing a salt concentration in electrolytes increased electrolyte viscosity and resulted in the formation of a thicker, yet smoother SEI on a Li foil anodes. Most cathodes showed the most favorable performance in a 3 M electrolyte at 70 °C with S-YP17D retaining over 450 mAh g_s^{-1} at C/5 rate after 100 cycles. Increasing salt concentration from 3 M to 5 M reduced accessible capacity in microporous S-YP17D even at a moderate C/5 rate, but had little effect on the accessible capacity of mesoporous S-AC samples. Higher electrolyte molarity also resulted in more polysulfides being re-deposited on the surface of S-AC particles, likely due to lower polysulfide solubility and slower transport in electrolytes having higher salt concentration. The studies of voltage profiles during cycling show that increasing the S-AC particles size and increasing electrolyte molarity results in the significant polarization.

Acknowledgments

This work was supported by the Energy Efficiency & Resources program of the Korea Institute of Energy Technology Evaluation and Planning (KETEP) funded by the Korea government Ministry of Knowledge Economy (grant 20118510010030) and by the US Army Research Office (grant W911NF-12-1-0259).

References

[1] B. Scrosati, J. Hassoun, Y.-K. Sun, Energy Environ. Sci. 4 (9) (2011) 3287–3295.
[2] J.B. Goodenough, Y. Kim, J. Power Sources 196 (16) (2011) 6688–6694.
[3] N.S. Choi, et al., Angew. Chem. Int. Ed. 51 (40) (2012) 9994–10024.
[4] E.J. Cairns, H. Shimotake, Science 164 (1969) 1347–1355.
[5] J.T. Kummer, N. Weber, A Sodium–Sulfur Secondary Battery, Society of Automotive Engineers, 1967.
[6] D. Peramunage, S. Licht, Science 261 (5124) (1993) 1029–1032.
[7] R. Rauh, et al., J. Electrochem. Soc. 126 (4) (1979) 523–527.
[8] M.-K. Song, E.J. Cairns, Y. Zhang, Nanoscale (2013).
[9] X. Ji, et al., Nat. Commun. 2 (2011) 325.
[10] P.G. Bruce, et al., Nat. Mater. 11 (1) (2012) 19–29.
[11] X. Ji, K.T. Lee, L.F. Nazar, Nat. Mater. 8 (6) (2009) 500–506.
[12] J.-W. Choi, et al., Electrochim. Acta 52 (5) (2007) 2075–2082.
[13] J.H. Shin, E.J. Cairns, J. Power Sources 177 (2) (2008) 537–545.
[14] S.S. Jeong, et al., J. Power Sources 174 (2) (2007) 745–750.
[15] J. Hassoun, B. Scrosati, Angew. Chem. Int. Ed. 49 (13) (2010) 2371–2374.
[16] E.S. Shin, K. Kim, S.H. Oh, W.I. Cho, Chem. Commun. 49 (20) (2013) 2004–2006.
[17] L. Suo, et al., Nat. Commun. 4 (2013) 1481.
[18] J.T. Lee, et al., Adv. Mater. 25 (33) (2013) 4573–4579.
[19] E. Peled, et al., J. Power Sources 26 (3–4) (1989) 269–271.
[20] S. Kim, Y.J. Jung, H.S. Lim, Electrochim. Acta 50 (2–3) (2004) 889–892.
[21] D. Aurbach, et al., J. Electrochem. Soc. 156 (8) (2009) A694–A702.
[22] Z. Lin, et al., Adv. Funct. Mater. (2012).
[23] R. Elazari, et al., Adv. Mater. 23 (47) (2011) 5641.
[24] J.L. Wang, et al., Adv. Mater. 14 (13–14) (2002) 963.
[25] Y. Yang, et al., ACS Nano 5 (11) (2011) 9187–9193.
[26] L. Ji, et al., J. Am. Chem. Soc. 133 (46) (2011) 18522–18525.
[27] C. Barchasz, et al., J. Power Sources 211 (0) (2012) 19–26.
[28] H. Kim, J.T. Lee, G. Yushin, J. Power Sources 226 (0) (2013) 256–265.
[29] M. Xiao, et al., RSC Adv. 3 (15) (2013) 4914–4916.
[30] N. Jayaprakash, et al., Angew. Chem. Int. Ed. 50 (26) (2011) 5904–5908.
[31] Y. Yang, et al., Nano Lett. 10 (4) (2010) 1486–1491.
[32] B. Zhang, et al., Energy Environ. Sci. 3 (10) (2010) 1531–1537.
[33] Y. Fu, A. Manthiram, J. Phys. Chem. C 116 (16) (2012) 8910–8915.
[34] J.C. Guo, Y.H. Xu, C.S. Wang, Nano Lett. 11 (10) (2011) 4288–4294.
[35] L. Xiao, et al., Adv. Mater. 24 (9) (2012) 1176–1181.
[36] L. Ji, et al., Energy Environ. Sci. 4 (12) (2011) 5053–5059.
[37] E.N. Hoffman, et al., Microporous Mesoporous Mater. 112 (1–3) (2008) 526–532.
[38] Y. Korenblit, et al., Adv. Funct. Mater. 22 (8) (2012) 1655–1662.
[39] K. Evanoff, et al., Adv. Mater. 24 (4) (2012) 533.
[40] M. Rose, et al., Small (2011) 1108–1117.
[41] L. Wei, N. Nitta, G. Yushin, ACS Nano 7 (8) (2013) 6498–6506.
[42] L. Wei, et al., Adv. Funct. Mater. 22 (4) (2012) 827–834.
[43] L. Wei, et al., Adv. Energy Mater. 1 (2011) 356–361.
[44] I.T. Kim, et al., Carbon 52 (2013) 56–64.
[45] A. Magasinki, et al., ACS Appl. Mater. Interfaces 2 (11) (2010) 3004–3010.
[46] D.E. Sands, J. Am. Chem. Soc. 87 (6) (1965) 1395–1396.
[47] T. Frauenheim, et al., J. Non-Cryst. Solids 182 (1) (1995) 186–197.
[48] N. Setoyama, T. Suzuki, K. Kaneko, Carbon 36 (10) (1998) 1459–1467.
[49] Ö. Polat, et al., Mater. Res. Bull. 48 (2) (2013) 352–356.
[50] C. Liang, N.J. Dudney, J.Y. Howe, Chem. Mater. 21 (19) (2009) 4724–4730.
[51] Y.V. Mikhaylik, J.R. Akridge, J. Electrochem. Soc. 151 (11) (2004) A1969–A1976.